Published in "Physical Chemistry Chemical Physics 15(33): 13902–13910, 2013"
which should be cited to refer to this work.

Ligand field density functional theory calculation of the $4f^2 \rightarrow 4f^15d^1$ transitions in the quantum cutter $Cs_2KYF_6:Pr^{3+}$

Harry Ramanantoanina,[a] Werner Urland,*[ab] Fanica Cimpoesu*[c] and Claude Daul*[a]

Herein we present a Ligand Field Density Functional Theory (LFDFT) based methodology for the analysis of the $4f^n \rightarrow 4f^{n-1}5d^1$ transitions in rare earth compounds and apply it for the characterization of the $4f^2 \rightarrow 4f^15d^1$ transitions in the quantum cutter $Cs_2KYF_6:Pr^{3+}$ with the elpasolite structure type. The methodological advances are relevant for the analysis and prospection of materials acting as phosphors in light-emitting diodes. The positions of the zero-phonon energy corresponding to the states of the electron configurations $4f^2$ and $4f^15d^1$ are calculated, where the praseodymium ion may occupy either the Cs^+-, K^+- or the Y^{3+}-site, and are compared with available experimental data. The theoretical results show that the occupation of the three undistorted sites allows a quantum-cutting process. However size effects due to the difference between the ionic radii of Pr^{3+} and K^+ as well as Cs^+ lead to the distortion of the K^+- and the Cs^+-site, which finally exclude these sites for quantum-cutting. A detailed discussion about the origin of this distortion is also described.

Introduction

After the ban on incandescent light bulbs, which consume about 90% of the incoming energy as heat, mankind is nowadays looking for another light source for white light or even better warm-white light. Artificial white light is yet mainly obtained by the combination of a GaN blue light-emitting diode (LED) with an inorganic yellow phosphor. A good phosphor should absorb the excitation energy and emit light afterwards as efficiently as possible, insofar as the quantum efficiency is maximized. Furthermore the elapsed time between the excitation and the emission should be very short to avoid afterglow. In order to meet these conditions, transitions with high transition probabilities and short lifetimes are needed. These criteria are best achieved by means of lanthanide ions in various host lattices showing the $4f^n \rightarrow 4f^{n-1}5d^1$ transitions.[1] A good yellow phosphor for producing white light with a blue LED is for instance $Y_3Al_5O_{12}$ (YAG) doped with Ce^{3+} ions.[2] This LED has been broadly used as a long-life white-light source in traffic lights, cycle lamps, car headlights, outdoor lighting, flashlights or marking lamps in tunnels. However the generated light looks so far bluish cold.

The concept of warm-white light requires a LED coated with two or three phosphors, where at least one of them should emit red light leading to the warm impression.

In order to find more appropriate phosphors than those already in use and in order to avoid somehow laborious and time-consuming trial-and-error experiments, theoretical modelling of the structure of the compounds and theoretical prediction of the corresponding electronic structure and optical properties are necessary.

Theoretical prediction of the spectroscopic properties of lanthanide ions is important since they are involved in the design of good phosphors. Semi-empirical computational models are available,[3–7] which allow us to determine the electronic structure of trivalent lanthanide ions in various host lattices, even though their application remains limited by symmetry constraints.[4–7] Full *ab initio* wave function theory models also exist.[8] The quantum chemistry of lanthanides is being non-trivial as a consequence of some technical problems such as the non-aufbau nature of the f-orbitals.[9–12] On the other hand, Density Functional Theory (DFT) models can be applied routinely to medium-to-large-size compounds. Therefore DFT is nowadays becoming very popular amongst the computational chemists community.[13]

[a] *Department of Chemistry of the University of Fribourg, Chemin du Musée 9, 1700 Fribourg, Switzerland. E-mail: claude.daul@unifr.ch; Fax: +41 26 300 9738; Tel: +41 26 300 8700*
[b] *Institut für Anorganische Chemie der Universität Hannover, Callinstr. 9, D-30167 Hannover, Germany. E-mail: wurland@arcor.de*
[c] *Institute of Physical Chemistry, Splaiul Independentei 202, Bucharest 060021, Romania. E-mail: cfanica@yahoo.com*

DFT can in principle be used to calculate optical properties of materials,[14–16] *e.g.* using TDDFT[17,18] or Delta-SCF.[19,20] However, combining classical ligand field theory[21,22] or, in a certain context, crystal field theory with DFT gives rise to interesting results with a relatively good agreement with the experimental data. We developed the concept of a multideterminental DFT, based on the association of ligand field theory and DFT, forming the acronyms LFDFT.[23,24] The analysis of the single open-shell transition metal d-electrons[25–27] or the lanthanide f-electrons[25,28–30] is well established and currently practiced, while the consideration of the two-open-shells, *i.e.* f- and d-electrons, is a challenge solved in the present work. With this model, it is possible to predict new quantum cutters with praseodymium ions,[31,32] which are doped into different solids like fluorides, chlorides, oxides, *etc.*, capable of emitting more than one visible photon after the absorption of a single high-energy photon. Accordingly, a quantum efficiency of more than 100% is expected and in the special case of Pr^{3+}, one photon is emitted in the orange-red region,[1] making it important to the design of warm-white light phosphors.

Herein we report the analysis of Pr^{3+}, characterized by the $4f^2$ and $4f^15d^1$ electron configurations, doped in Cs_2KYF_6 crystallizing in the elpasolite structure type. Schiffbauer *et al.*[33] have found experimentally that this compound shows quantum-cutting, although their theoretical conclusions might be a subject of discussion. The elpasolite structure type represents a cubic closest packing of Cs^+ and F^- ions, where the octahedral voids formed by the F^- ions are filled by Y^{3+} and K^+ ions, while the Cs^+ ions are coordinated by 12 F^- ions forming a cubo-octahedral environment (*cf.* Fig. 1). The LFDFT model takes into account the 91 microstates corresponding to the $4f^2$ ground electron configuration and the 140 microstates of the excited $4f^15d^1$ electron configuration of Pr^{3+} considering the inter-electronic effect, the spin–orbit coupling and the influence of the ligand field in a non-empirical way. To be a quantum cutter, the highest state corresponding to the $4f^2$ configuration, the $^1S_0$ term, should lie below the lowest level of the excited $4f^15d^1$ configuration, avoiding an overlap of both electronic configurations. Our non-empirical calculations do not confirm the conclusions of Schiffbauer *et al.*[33] Although reliable in the general account of a crystal as a whole, the Schiffbauer *et al.*[33] calculations, based on plane waves and empirical relationships, cannot account for details related to lanthanide ion configurations and ligand field issues, as presented in our analysis. Also their model does not make explicit the possibility of lattice disorder or local disorder,[34] which cannot be ruled out, as a matter of principle, when we consider the case of doped materials.

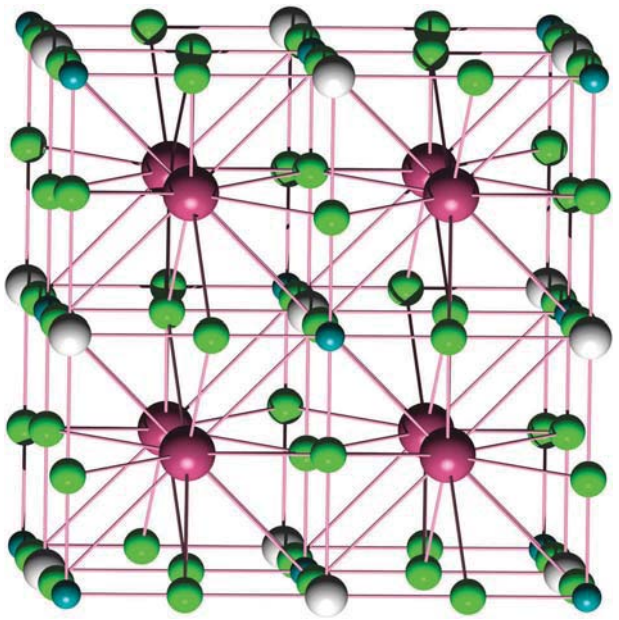

Fig. 1 Spatial representation of the unit cell of Cs_2KYF_6 elpasolite type structure. Colour code: F^- in green, Y^{3+} in blue, K^+ in white and Cs^+ in red.

Methodology

The LFDFT approach

The theory of the ligand field and the concept of the LFDFT are exhaustively explained elsewhere.[21–24] Herein, we are just giving a brief summary of the general methodology. The LFDFT model, which includes two-open-shells f- and d-electrons presented here, is an extension of the previously published models being successfully applied to the physical properties of transition metals[25–27] or lanthanide complexes.[25,28–30]

In LFDFT, the central Pr^{3+} ion is subjected to a perturbation due to the surrounding ligands. The Hamiltonian which describes such a system is represented in terms of two-electron repulsion integrals, one electron ligand field and spin–orbit coupling parameters within the manifold of the $4f^2$ and $4f^15d^1$ electron configurations (eqn (1)).

$$\boldsymbol{H} = \boldsymbol{H}_{\mathbf{EE}} + \boldsymbol{H}_{\mathbf{LF}} + \boldsymbol{H}_{\mathbf{SO}} \quad (1)$$

where $\boldsymbol{H}_{\mathbf{EE}}$, the Hamiltonian corresponding to the two-electrons effect, is treated as atomic-like perturbation, which preserves the spherical symmetry. This interaction yields 7 spectroscopic terms of the $4f^2$ electron configuration (eqn (2)) and 10 spectroscopic terms of the $4f^15d^1$ excited electron configuration (eqn (3)).

$$f^2 \rightarrow {}^1S + {}^3P + {}^1D + {}^3F + {}^1G + {}^3H + {}^1I \quad (2)$$

$$f^1d^1 \rightarrow {}^1P + {}^3P + {}^1D + {}^3D + {}^1F + {}^3F + {}^1G + {}^3G + {}^1H + {}^3H \quad (3)$$

The $\boldsymbol{H}_{\mathbf{EE}}$ matrix elements are calculated within the basis of Slater determinants, using the well known Slater's rules,[21] and can be expressed in terms of 10 Slater–Condon parameters[21] such as the direct Slater parameters for the direct Coulomb interaction: $F_k(ff)$ and $F_k(fd)$, where k = 0, 2, 4 and 6 for the $4f^2$ electron configuration and k = 0, 2, 4 for the $4f^15d^1$ electron configuration, respectively, and the exchange interaction within the $4f^15d^1$ electron configuration, $G_k(fd)$, where k = 1, 3 and 5.

$\boldsymbol{H}_{\mathbf{LF}}$, the Hamiltonian corresponding to the ligand field potential, takes full account for the lowering of the symmetry due to the chemical environment of the Pr^{3+} ion center. Within the manifold of 4f- and 5d-orbitals, the 12 × 12 matrix that corresponds to the ligand field potential is then presented as follows:

$$\boldsymbol{H}_{\mathbf{LF}} = \begin{pmatrix} \boldsymbol{H}_{\mathbf{LF}}(\mathbf{f}) & \boldsymbol{H}_{\mathbf{LF}}(\mathbf{fd}) \\ \boldsymbol{H}_{\mathbf{LF}}(\mathbf{fd})^{T*} & \boldsymbol{H}_{\mathbf{LF}}(\mathbf{d}) \end{pmatrix} \tag{4}$$

where $\boldsymbol{H}_{\mathbf{LF}}(\mathbf{f})$ and $\boldsymbol{H}_{\mathbf{LF}}(\mathbf{d})$ are 7 × 7 and 5 × 5 block matrices, which represent the splitting of the 4f and 5d orbital energies due to the ligand field, respectively.

The off-diagonal 7 × 5 block matrix $\boldsymbol{H}_{\mathbf{LF}}(\mathbf{fd})$ can be assigned to 0 by symmetry, if the chemical environment exhibits an inversion center (*e.g.* in this case O_h), where f and d atomic bases possess opposite parity. For systems with lower symmetry, the off-diagonal $\boldsymbol{H}_{\mathbf{LF}}(\mathbf{fd})$ block can be conceived as negligible in perturbation effects, for the reason that its conceivably small elements are superseded by the large f–d gap. However, the non-diagonal f–d block can be easily handled within the model we propose. In an octahedral ligand field this interaction, for instance, splits the ground state ^3H (eqn (2)) of the Pr^{3+} ion into 4 triplet electronic states representative of the irreducible representation (irreps) of the O_h point group (eqn (5)).

$$^3H \rightarrow {}^3E_u + {}^3T_{1u} + {}^3T_{1u} + {}^3T_{2u} \tag{5}$$

The ligand field matrices $\boldsymbol{H}_{\mathbf{LF}}(\mathbf{f})$, $\boldsymbol{H}_{\mathbf{LF}}(\mathbf{d})$ and $\boldsymbol{H}_{\mathbf{LF}}(\mathbf{fd})$ are mostly constructed on the basis of spherical harmonics functions $Y_{k,q}$ as described in eqn (6).[35]

$$\boldsymbol{H}_{\mathbf{LF}}(\mathbf{f}) = \sum_{k=2,4,6} \sum_{q=-k}^{k} B_q^k(\mathrm{f}) C_q^{(k)} \tag{6a}$$

$$\boldsymbol{H}_{\mathbf{LF}}(\mathbf{d}) = \sum_{k=0,2,4} \sum_{q=-k}^{k} B_q^k(\mathrm{d}) C_q^{(k)} \tag{6b}$$

$$\boldsymbol{H}_{\mathbf{LF}}(\mathbf{fd}) = \sum_{k=1,3,5} \sum_{q=-k}^{k} B_q^k(\mathrm{fd}) C_q^{(k)} \tag{6c}$$

where B_q^k, the Wybourne parameters,[35] are in general complex numbers, which act as one-electron parameters in front of solid spherical harmonic operators (eqn (7)).

$$C_q^{(k)} = \sqrt{\frac{4\pi}{2k+1}} Y_{k,q} \tag{7}$$

It is noteworthy that the $\boldsymbol{H}_{\mathbf{LF}}(\mathbf{f})$ expansion excludes by convention the $k = 0$ term, being a traceless block, as usual for one-open-shell ligand field problems, but the $\boldsymbol{H}_{\mathbf{LF}}(\mathbf{d})$ must include a $k = 0$ term (*i.e.* a $B_0^0(\mathrm{d})$ parameter) responsible for the 4f–5d orbital gap. The $\boldsymbol{H}_{\mathbf{LF}}(\mathbf{fd})$ matrix has odd parity due to the symmetry of the f ⊗ d product, being expanded with corresponding $k = 1$, 3 and 5 solid spherical harmonics.

This formulation of the ligand field potential (eqn (6)) and related representation are like the Stevens parameters $A_{k,q}$,[35,36] while elegant might be sometimes cumbersome and does not offer any chemical insight. To circumvent this problem, we have decided to represent our ligand field potential using the so-called Angular Overlap Model (AOM),[37] inasmuch as in each computational step we are performing, its plausibility connected with chemical insight is given. The theory of AOM is also exhaustively explained elsewhere[37,38] and was applied thoroughly to describe the influence of the ligand field on either the 3d-orbital of the transition metal[37] or the 4f-orbital of lanthanide complexes.[3] The AOM approach represents the 7 × 7 $\boldsymbol{H}_{\mathbf{LF}}(\mathbf{f})$ and the 5 × 5 $\boldsymbol{H}_{\mathbf{LF}}(\mathbf{d})$ ligand field matrices in terms of two different sets of e_σ and e_π parameters for each ligand donor, weighted by factors depending to the angular position of the ligand in the coordination sphere of the Pr^{3+} center. The e_σ and e_π parameters, which are proper to a specific ligand, obviously represent the power of the ligand to be a σ- or a π-donor, making them useful while we compare our results to the experimental data. Thus we have fitted our DFT calculated $\boldsymbol{H}_{\mathbf{LF}}$ to the AOM parameters.

$\boldsymbol{H}_{\mathbf{SO}}$, the Hamiltonian corresponding to the spin–orbit coupling is important because of the large spin–orbit coupling constant encountered in the praseodymium atom, *i.e.* ζ_{4f} = 731 cm^{-1} and ζ_{5d} = 1012 cm^{-1} observed experimentally.[5,39] Therefore, the inclusion of the spin–orbit coupling is also performed in the model. Due to this interaction, the orbital multiplets obtained so far (eqn (5), parity is omitted for convenience) are further split into spin–orbit components representative of the irreps of the O* double group (eqn (8)).

$$^3E \rightarrow \Gamma_4 + \Gamma_5$$

$$^3T_1 \rightarrow \Gamma_1 + \Gamma_3 + \Gamma_4 + \Gamma_5$$

$$^3T_2 \rightarrow \Gamma_2 + \Gamma_3 + \Gamma_4 + \Gamma_5 \tag{8}$$

The LFDFT calculation presented here involves three steps: (i) an Average of Configuration (AOC) with equal occupation of the 4f-orbital and 5d-orbital is carried out. An AOC calculation is a molecular DFT calculation, which takes into account all interactions, *i.e.* overlap, electrostatic,... between the metal center and the ligands. Furthermore, it is always observed from the population analysis of the Kohn–Sham frontier orbitals that they are mostly constructed (over 95%) by the 3d-atomic orbital of the transition metal ion[25–27] or the 4f-atomic orbital of the lanthanide ion,[25,28–30] giving further evidence for the analysis of the ligand field by perturbation theory. (ii) While these orbitals are kept frozen, the energies of all single determinants (SD) within the whole ligand field manifold are performed, *i.e.* the 91 microstates of the $4f^2$ and 140 microstates of the $4f^15d^1$ electron configurations. These energies are then used to estimate the 10 Slater–Condon parameters and the ligand field potential needed in the present model using a least squares fit procedure. (iii) The multiplet splitting of $4f^2$ and the $4f^15d^1$ electron configurations is then calculated by diagonalizing the Hamiltonian $\boldsymbol{H}$ given in eqn (1), having the series of 231 Slater determinants as a basis.

Computational details

The DFT calculations reported in this paper have been carried out by means of the Amsterdam Density Functional (ADF2010) program package.[40–42] The local density approximation (LDA) characterized by the Vosko–Wilk–Nussair parameterization[43] of the electron gas, as well as the generalized gradient approximation (GGA) based on the OPBE parameterization[44] and the hybrid B3LYP functional[45] have been used for the exchange–correlation energy and potential. The molecular orbitals were expanded using an uncontracted quadruple-ζ STO basis sets plus one polarization function (QZ4P) for the F and Pr atoms. The standard LFDFT software running in the Matlab/Octave environment has been developed in Fribourg during the last two decades. It is freely available from the authors upon request.

The geometries of the three undistorted sites (Y^{3+}-, K^{+}- and Cs^{+}-sites) were taken from the work of Schiffbauer *et al.*,[33] where the experimental bond lengths between the F^{-} ion and the Y^{3+}, K^{+} and Cs^{+} were 2.156 Å, 2.573 Å and 3.350 Å, respectively. When the Pr^{3+} ion is doped into these three sites, Schiffbauer *et al.*[33] calculated the bond lengths between the F^{-} ion and the Pr^{3+} ion by means of the VASP crystal structure[33,46] modelling and found 2.260 Å, 2.455 Å and 2.715 Å, respectively. Then we have taken the optimized geometry reported by Schiffbauer *et al.*,[33] especially for the case of Y^{3+}- and K^{+}-sites, where a slight breathing of the octahedral cage might be expected, whereas such a breathing of the high symmetry structure must be avoided for the large cubo-octahedral Cs^{+}-site, within the T_d point group. Hence in the case of the occupation of the Cs^{+}-site, only off-center relaxation of the position of Pr^{3+} is permitted, while the position of the F^{-} ligands kept frozen to the experimental coordinates. This distortion follows either a tetragonal or a trigonal route leading to the formation of more stable structures, which belong to the C_{2v} and C_{3v} point groups, respectively. Positive point charges are added to mimic a Madelung potential, which neutralize the highly negatively charged structures. The point charges are placed around the selected molecular structure, in the position of the next nearest neighbours using the Efield keyword available in the ADF program package.[40–42]

The calculation of the multiplet energies of the electron configurations $4f^2$ and $4f^15d^1$ of the Pr^{3+} ion was carried out using the geometries given above, making the assumption that excitation state does not exhibit any further structural relaxation.

Results and discussion

The electron configuration $4f^2$ of Pr^{3+} has been studied experimentally by several authors.[47–49] It is known that the atomic emission spectroscopy of the $4f^2$ configuration shows 12 known levels in the Pr^{3+} ion, where fitted Slater–Condon parameters, and many others are calculated showing a root mean square of a magnitude of the wave number.[50] The energy level corresponding to the highest state $^1S_0$ was not observed for a long time. To date, it has been reasonably measured to be about 48 000 cm^{-1}.[51] The excited electron configuration $4f^15d^1$ has also been studied,[49,52] and in the emission spectroscopy, exactly 20 energy levels are observed. The energies corresponding to those spectroscopic terms are reported within the framework of the National Institute of Standards and Technologies (NIST) database.[52,53] The splitting of this excited electron configuration ($4f^15d^1$) due to the spin–spin and the spin–orbit couplings is determined to be about 18 000 cm^{-1}.[52,53] Using LFDFT, the energies of the 231 Slater determinants (91 for the $4f^2$ and 140 for the $4f^15d^1$ electron configurations) are calculated, which allows us to fit them to the $\boldsymbol{H}_{\mathbf{EE}}$ matrix elements and finally to extract 10 Slater–Condon parameters with a relatively small root mean square deviation. These parameters are presented in Table 1, together with the fitted parameters out of the multiplet splitting given in the NIST database.[52,53]

The free ion spectral terms (eqn (2) and (3)) are determined, aside from the two-electron parameters by a one-electron part that implies a gap between the energies of 4f- and 5d-orbitals. Thus all the terms originating from $4f^2$ (eqn (2)) imply a $2h_f$ one-electron, *i.e.* a kinetic plus electron-nuclear part, while those originating from $4f^15d^1$ (eqn (3)) contain a $h_f + h_d$ one electron amount. The $F_k(ff)$ parameters with $k > 0$ determine the split of the terms, since all the $4f^2$ configurations have a common $F_0(ff)$ amount, or in other words, the $F_0(ff)$ does not contribute to the split. Similarly, the $4f^15d^1$ multiplets are determined by $F_k(fd)$ with $k > 0$ and $G_k(fd)$, the zero order $F_0(fd)$ quantity being the same for all the $4f^15d^1$ terms. Therefore the $\Delta_0(fd)$ parameter in Table 1 is composed of different parameters, which cannot be discriminated separately, eqn (9).

$$\Delta_0(fd) = h_f - h_d + F_0(fd) - F_0(ff) \quad (9)$$

The $F_0(ff)$ parameter is conventionally fixed to zero without impinging upon the ligand field analysis. From Table 1, we can calculate the splitting of the $4f^2$-, which represents the energy of the highest $^1S_0$ state and the $4f^15d^1$-electron configuration in terms of the calculated Slater–Condon parameters, including the spin–orbit coupling. The values for the energy of the $^1S_0$ electronic state are determined, even though the term is hardly

Table 1 Fitted Slater–Condon parameters (in cm^{-1}) obtained for Pr^{3+} for the $4f^2$ ($F_k(ff)$) and $4f^15d^1$ electron configurations ($F_k(fd)$ and $G_k(fd)$), using the LDA, the GGA and the hybrid DFT functionals

	LDA	GGA	Hybrid	Exp.[a]
$F_0(ff)$	0.0	0.0	0.0	0.0
$F_2(ff)$	377.4	388.2	382.4	316.7
$F_4(ff)$	26.8	33.1	30.7	58.7
$F_6(ff)$	4.5	5.3	3.0	5.5
$\Delta_0(fd)$	56100.7	57804.6	54325.3	54701.7
$F_2(fd)$	280.4	290.1	275.2	222.0
$F_4(fd)$	21.3	22.1	16.8	30.0
$G_1(fd)$	69.6	68.9	95.4	326.1
$G_3(fd)$	44.3	43.0	36.5	34.5
$G_5(fd)$	9.7	9.7	10.9	7.4

[a] These parameters are fitted to the energy levels given in the NIST database (ref. 53).

visible in the experimental spectroscopy.[51] It was found to be 49 372 cm^{-1}, 53 082 cm^{-1} and 48 154 cm^{-1}, respectively, while the LDA, GGA and B3LYP were used in the DFT calculation as functionals. At the same time, the splitting of the energy levels corresponding to the $4f^15d^1$ electron configuration are calculated to be 20 995 cm^{-1}, 21 353 cm^{-1} and 20 125 cm^{-1} by the LDA, GGA and B3LYP calculation, respectively. Accordingly, the DFT calculation, where the B3LYP functional is used, is most appropriate to represent the atomic spectroscopy of the ground $4f^2$ and excited $4f^15d^1$ electron configurations of Pr^{3+} ions.

While the Pr^{3+} ion is doped into the host lattices composed of F^- ligands, the effect of the ligand field is included in the Hamiltonian and splits the multiplet obtained for the free ion into various ligand field energy levels. In contrast to the situation in transition metal d-electrons, where the Racah parameters obtained for the free ion are drastically reduced in the presence of a ligand field,[54,55] the Slater–Condon parameters calculated for the free ion change slightly.

In the Cs_2KYF_6 elpasolite structure type, the Pr^{3+} ion may occupy either the octahedral Y^{3+}- and the K^+-site, or the large cubo-octahedral Cs^+-site. The geometry of these three different sites are obtained from the work of Schiffbauer *et al.*[33] We accept their optimized geometry in the case of the Y^{3+}- or the K^+-site, where the experimental distances between Pr^{3+} and F^- either elongates from 2.156 Å to 2.260 Å or compresses from 2.573 Å to 2.455 Å. We strongly reject their conclusion in the case of the experimentally large Cs^+-site. Indeed, despite the fact that a trivalent Pr ion is most unlikely to replace a monovalent ion due to the crystal disorder induced, we claim that the doping of the large Cs^+-site will lead to an off-center displacement of the Pr^{3+} ion, lowering the previously high ligand field symmetry. Thus the distortion of the large Cs^+-site is important when Pr^{3+} is doped in the considered site.

The calculation of Schiffbauer *et al.*[33] takes into account only the totally-symmetric displacement of the fluoride cage, whereas it is observed from the scanning of the potential energy surface in Fig. 2 that the relaxation of the position of Pr^{3+}, while the positions of F^- ions are kept frozen to the experimental coordinates, goes for the Cs^+-site always along a trigonal distortion towards three F^- ligands which form an equilateral triangle. Finally the Pr^{3+} ion makes a short contact with these three F^- ions, where bond lengths of about 2.233 Å were calculated. This new bond length formed between Pr^{3+} and three F^- ligands corresponds to an off-center displacement of the Pr^{3+} ion of about 1.619 Å. It is noteworthy that this bond length stabilizes the ionic arrangement, which belongs to the C_{3v} point group (Fig. 2). Therefore we have taken this optimized arrangement for the calculation of the multiplet energy splitting given in Fig. 3f. Because of the large experimental bond length determined between K^+ and F^- ions, *i.e.* 2.573 Å,[33] an off-center displacement of the Pr^{3+} ion is also expected when the Pr^{3+} ion is doped in the K^+-site. Although Schiffbauer *et al.*[33] have not considered this hypothesis, we have constructed the geometry of the Pr^{3+} ion in an off-center octahedral ligand environment, in which coordinates are frozen to the

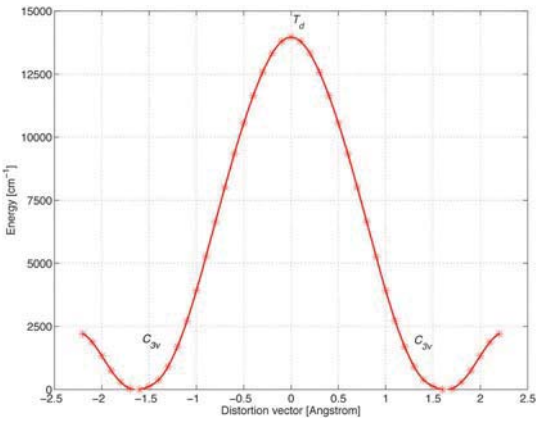

Fig. 2 DFT scan of the potential energy profile for the off-center displacement of the Pr^{3+} ion along the C_3 axis in the case of the occupation of Cs^+-site.

experimental data, insofar as the bond lengths between the Pr^{3+} ion and the nearest F^- ligands match 2.2 Å, in accordance with the Shannon radii[56] corresponding to Pr^{3+} and F^- in such a type of coordination. Hence the multiplet energy splitting, while this hypothetical but yet probable geometry is taken into account, is calculated and shown in Fig. 3e.

The study of the electronic structure of lanthanide complexes by AOM is not as popular as the study of transition metal compounds. So far literature data have been quite limited and become even more sparse when dealing with more complicated ligands. However AOM has the advantage to give a certain chemical intuitiveness to reject or not the theoretical prediction, giving a further insight into the feasibility of the prediction of quantum cutter. In Table 2, we present the AOM parameters according to the choice of exchange–correlation functional used along with the LFDFT procedure in the case of the doping of the Y^{3+}-site. The AOM parameters are obtained by fitting the LFDFT $\boldsymbol{H}_{\mathbf{LF}}$ potential to the AOM matrix[3,37] using a least squares fit procedure. Two parameters e_σ and e_π are involved for the ligand fields of the 4f- and 5d-electrons, respectively.

The eigenvalues of the $\boldsymbol{H}_{\mathbf{LF}}$ matrix give the energy splitting of the 4f and 5d orbitals of the Pr^{3+} ion within the ligand field. By means of the AOM parameters presented in Table 2, it is possible to make a direct calculation of those eigenvalues without performing a diagonalization procedure of the 12 × 12 $\boldsymbol{H}_{\mathbf{LF}}$ matrix. Hence in the octahedral ligand field, the f-orbital splits into a_{2u}, t_{2u} and t_{1u}, whose energies can be calculated as 0, $(5/2)e_\pi(f)$ and $2e_\sigma(f) + (3/2)e_\pi(f)$, respectively. Using the same approach, the d-orbital splits into t_{2g} and e_g, whose energies can be calculated as $B_0{}^0(d) + 4e_\pi(d)$ and $B_0{}^0(d) + 3e_\sigma(d)$, respectively. Moreover, a possibility to make a connection between the AOM and the Wybourne-normalized crystal field parameters for f- and d-electrons can be found in ref. 3 and 37, respectively. For the special case of O_h ligand field, this connection can be determined (eqn (10)).

$$B_0{}^4(f) = \frac{3}{2}(3e_\sigma(f) + e_\pi(f)) \qquad (10a)$$

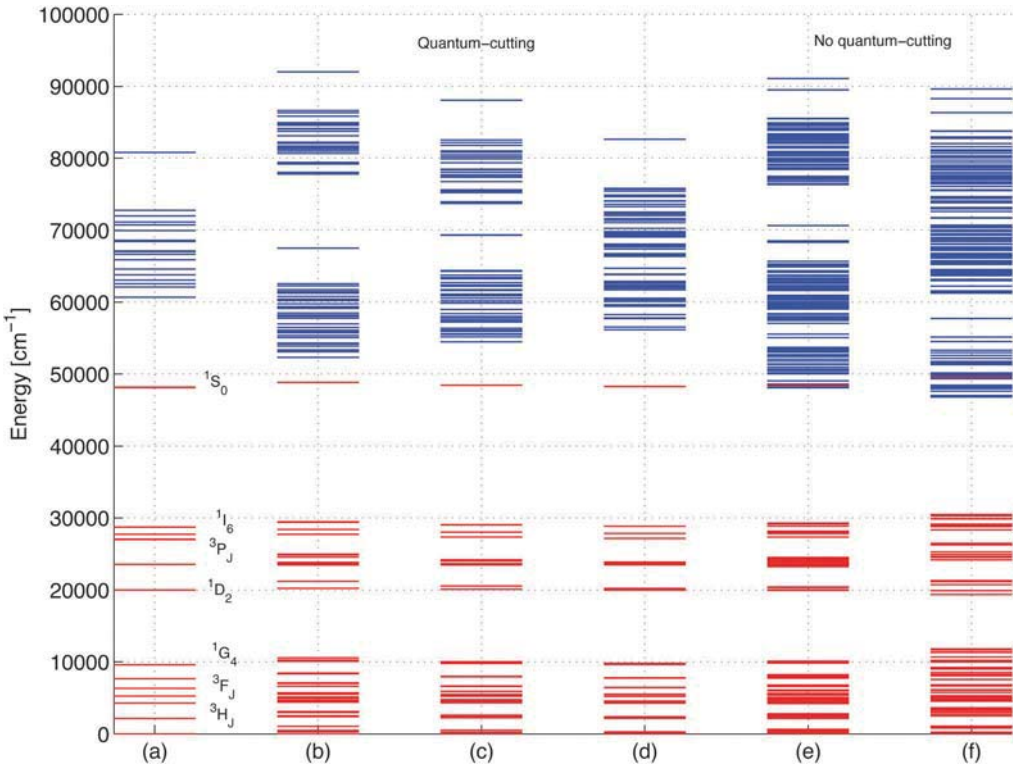

Fig. 3 LFDFT multiplet energies calculated at the B3LYP level of theory, corresponding to the $4f^2$ (in red) and $4f^15d^1$ electron configurations (in blue): for the free Pr^{3+} ion (a); doping of the Y^{3+}-site (b), the K^+-site (c) and the Cs^+-site (d), where the coordinates are taken as the optimized geometries from the work of Schiffbauer *et al.*;[33] doping of the K^+-site (e) and Cs^+-site (f) with the off-center displacement of the Pr^{3+} ion. The multiplet states of the $4f^2$-electron configuration of the free ion are highlighted.

Table 2 Calculated AOM parameters (cm^{-1}) fitted to the ligand field potential of the Pr^{3+} ion doped into the Y^{3+}-site obtained in the LFDFT, using the LDA, GGA and hybrid functional

Y^{3+}-site	$e_\sigma(f)$	$e_\pi(f)$	$e_\sigma(d)$	$e_\pi(d)$
LDA	1222.5	531.9	15230.5	5498.6
GGA	1337.0	559.4	14408.9	5372.3
Hybrid	641.7	344.6	15252.4	5307.7

$$B_0{}^6(f) = \frac{39}{56}(2e_\sigma(f) - 3e_\pi(f)) \qquad (10b)$$

$$B_0{}^4(d) = \frac{21}{10}(3e_\sigma(d) - 4e_\pi(d)) \qquad (10c)$$

From the spectroscopic measurements of Tanner *et al.*,[57] and experimental magnetic studies of Urland,[58] on the elpasolite Cs_2KPrF_6, the AOM parameter $e_\sigma(f)$ in the range of 700–800 cm^{-1} with an approximate ratio $e_\sigma(f)/e_\pi(f)$ of 3 could be deduced (eqn (10a) and (10b)). Additionally, Tanner *et al.*,[59] from spectroscopic measurements of Pr^{3+} in chloride elpasolite lattices found a ligand field parameter $B_0{}^4(d)$ of 42 357 cm^{-1}, which is directly related to $21Dq$. This energy, assuming that $e_\sigma(d)/e_\pi(d) = 3$, allows us to determine $e_\sigma(d)$ in this case to a value of 12 102 cm^{-1} (eqn (10c)). From Table 2, besides the f-orbitals where the LDA and GGA calculation overestimates the splitting pattern, the parameters obtained for the d-orbitals are in agreement with the experimental data, taking into account that a chloride ligand possesses a smaller $10Dq$ value than a fluoride ligand according to the spectroscopic series. It is noteworthy to highlight that the B3LYP based DFT calculation gives once again more accurate results. This is probably due to the reduction of the self-interaction error, which is inherent within the LDA and GGA functionals. Therefore we have chosen the hybrid functional for the calculation of the energy multiplet splitting presented in Fig. 3.

We present in Fig. 3a the multiplet energy splitting of the free Pr^{3+} ion for the $4f^2$ and $4f^15d^1$ electron configurations. The energies of the corresponding spectroscopic terms are in accordance with what we found from the literature,[52,53] except for the energy level of the $^3P_2$, $^3P_1$, $^3P_0$ and $^1I_6$ terms from the $4f^2$-electron configuration, where a shift of about 3000 cm^{-1} is noticed. This is directly related to the overestimation of the parameters $F_2(ff)$ by DFT (*cf.* Table 1). Schiffbauer *et al.*[33] (see Fig. 3 in ref. 33) measured the excitation spectrum of Cs_2KYF_6:Pr^{3+} at a temperature of 10 K monitoring the emission at 408 nm, where they found the quantum-cutting process. They observed a broad band splitting into five transition peaks, which were assigned to the $4f^2$ ($^3H_4$) → $4f^15d^1$ transitions of the Pr^{3+} ion. The energy width, *i.e.* the energy range of the peak occurrence, corresponding to this experimental excitation spectrum of Cs_2KYF_6:Pr^{3+} can be estimated in the range of 212–115 nm, *i.e.* 39 786 cm^{-1}. Within the LFDFT calculation,

the multiplet splitting corresponding to the Pr^{3+} ion doped in the Y^{3+}- (Fig. 3b), K^{+}- (Fig. 3c), and Cs^{+}-sites (Fig. 3d) obtained when the geometry was taken from the optimized coordinates of Schiffbauer *et al.*[33] exhibits the quantum-cutting process, as the highest electronic state $^1S_0$ of the $4f^2$ electron configuration always lies below the multiplets of the $4f^15d^1$ electron configuration. It is observed that the doping of these three sites allows us to characterize an interaction between the 5d-orbital and the ligands according to the strong-, the intermediate- and the weak-field for the case of the Y^{3+}-, the K^{+}- and the Cs^{+}-site, respectively. When the Pr^{3+} ion occupies the Y^{3+}-site (Fig. 3b), the energy width of the multiplet splitting of the $4f^15d^1$ electron configuration is calculated to be exactly 39 671 cm^{-1}, while that obtained for the case of the K^{+}-site (Fig. 3c) and the Cs^{+}-site (Fig. 3d), respectively, 33 598 cm^{-1} and 26 486 cm^{-1}, might be too low if compared to the experimental excitation spectrum. Moreover, Schiffbauer *et al.*[33] (see Fig. 4 in ref. 33) measured the high-resolution emission spectrum of Cs_2KYF_6:Pr^{3+} at 10 K and 180 nm excitation. The spectrum shows several sharp peaks corresponding to the $4f^2 \rightarrow 4f^2$ emission of Pr^{3+}. No broad peak characteristic of the $4f^15d^1 \rightarrow 4f^2$ emission is observed, in the meantime showing the experimental evidence of quantum-cutting. In the UV and visible regions of this spectrum, the transition assignment reported by Schiffbauer *et al.*[33] is mostly reproduced by the DFT calculation, more especially in the case of the doping of the Y^{3+}-site (Fig. 3b). By monitoring the emission at two different wavelengths, Schiffbauer *et al.*[33] (see Fig. 5 in ref. 33) measured the spectra, where a significant change in the shape of the spectra compared to the previous one is observed.[33] In these special cases, they concluded that no longer the quantum-cutting process is exhibited. Then the energy width corresponding to the splitting of the $4f^15d^1$ emission can be estimated to be 41 882 cm^{-1} and 44 052 cm^{-1}, respectively. These energies are much more larger in comparison to what we obtained for the three undistorted sites, suggesting that the Pr^{3+} ion is, in the presence of a very strong ligand field, even stronger than that occurring in the octahedral Y^{3+}-site. If we consider a distortion of the large K^{+}- and Cs^{+}-sites along a trigonal route, the quantum-cutting process is no longer retrieved (Fig. 3e and f). The Pr^{3+} ion comes closer towards three F^{-} ligands, eventually enhancing the splitting pattern of the 5d- as well as the 4f-orbital. Accordingly, the energy widths corresponding to the $4f^15d^1$ electron configuration for both cases are calculated to be 42 940 cm^{-1} and 42 802 cm^{-1}, respectively.

Schiffbauer *et al.*[33] have emphasized the assumption that in an octahedral ligand field, the d-orbital splits into e_g and t_{2g}, like the situation that appears in the excited $4f^05d^1$ electron configuration of the Ce^{3+} ion. They always referred to this particular situation through their description of the Pr^{3+} problem. Hence, for the description of the emission spectrum given in ref. 33 (see Fig. 5), they assume that the splitting of the emission spectra into two bands suggests the occupation of an O_h site. Therefore they conclude that neither the doping of the Y^{3+}-site nor the K^{+}-site show quantum-cutting because they exhibit a highly symmetrical environment with a relatively strong ligand field. Furthermore, they claim that the experimental excitation spectrum in ref. 33 (see Fig. 3) shows a weak ligand field with a low site symmetry because the broad band splits into five peaks, perhaps representative of the energy splitting of the 5d-orbitals due to a C_1 ligand field. Nevertheless, they came to the conclusion that the Pr^{3+} ion should be located on the large Cs^{+}-site allowing a weak ligand field, which in a certain way corroborates with their experimental observation. The spectroscopy of the excited $4f^15d^1$ electron configuration of Pr^{3+} ion is by far incompatible with that of the $4f^05d^1$ electron configuration in Ce^{3+} ion. The inter-electron effect already splits the $4f^15d^1$ electron configuration in five triplet and five singlet spectroscopic terms as shown in eqn (3), which are further split into numerous ligand field and spin–orbit component terms. While excited, all of these terms will be populated and emit photons afterwards at different levels of energy, regardless of the intensity of the corresponding emission.

Finally, we come to the conclusion that the emission spectrum reported by Schiffbauer *et al.*[33] measured in Fig. 3 of their paper represents the situation where the trivalent Pr ion is doped into the trivalent Y^{3+}-site, which allows quantum-cutting, as a result of both theoretical and experimental analysis.

Conclusions

In this paper, we present methodological advances tackling a rather complex problem of a ligand field accounting for 4f and 5d two-open-shell model Hamiltonian, focused on the interpretation and prospection of an important optical effect, the so-called quantum-cutting. In this respect, we used the frame of the original post-computational analysis algorithm named LFDFT for the simulation of the optical properties of the $4f^2$ and $4f^15d^1$ electron configurations of the trivalent praseodymium ion considering the following interaction: the inter-electron effects, the ligand field influence and the spin–orbit coupling parameters. Three different DFT settings, including LDA, GGA and the hybrid level of theory, are used along with the LFDFT procedure, where the B3LYP parameterization is found to be most suitable to represent the optical properties of the trivalent praseodymium ion. The theoretical calculations are meticulously verified and are presented in a way that a chemical insight is always given, *ergo* AOM parameterization of the ligand field is also performed.

By means of above mentioned procedures, the optical properties of Pr^{3+} doped into the Cs_2KYF_6 elpasolite type structure have been calculated. The theoretical calculations consider three types of situations, where the Pr^{3+} ion is doped into the Y^{3+}-site, the K^{+}-site and the Cs^{+}-site. It was shown that in these three situations, the calculated optical properties exhibit the quantum-cutting processes. Nevertheless this phenomenon is best achieved exclusively when the trivalent praseodymium ion is doped into the trivalent yttrium-site, since the doping of the K^{+}- and the large Cs^{+}-site generates an off-center displacement of the Pr^{3+} ion towards three fluoride ligands, *in fine* excluding these sites for quantum-cutting. The theoretical calculation was

compared to the experimental data, where emission and excitation spectra with a very good quality were available.

The theoretical prediction of the quantum-cutting processes is a valuable tool for the design of new phosphors. Since LFDFT is a fully non-empirical method, fast and accurate, it can be considered as a reliable tool for better understanding and further design of new quantum cutter materials.

Acknowledgements

This work is supported by the Swiss National Science Foundation. Support from the UEFISC-CDI research grant PCCE 9/2010 and travel grant ECOST-STSM-CM1002-151112-023359 from the Codecs program are also acknowledged.

Notes and references

1 H. A. Höppe, *Angew. Chem., Int. Ed.*, 2009, **48**, 3572.
2 S. Nakamura and G. Fasol, *The Blue Laser Diode*, Springer, Berlin, 1997.
3 W. Urland, *Chem. Phys.*, 1976, **14**, 393.
4 M. F. Reid, L. van Pieterson, R. T. Wegh and A. Meijerink, *J. Phys. Chem. B*, 2000, **62**, 14744.
5 M. Laroche, J.-L. Doualan, S. Girard, J. Margerie and R. Moncorgé, *J. Opt. Soc. Am. B*, 2000, **17**, 1291.
6 L. van Pieterson, M. F. Reid, R. T. Wegh, S. Soverna and A. Meijerink, *Phys. Rev. B: Condens. Matter Mater. Phys.*, 2002, **65**, 045113.
7 P. S. Peijzel, P. Vergeer, A. Meijerink, M. F. Reid, L. A. Boatner and G. W. Burdick, *Phys. Rev. B: Condens. Matter Mater. Phys.*, 2005, **71**, 045116.
8 J. L. Pascual, Z. Barandiaran and L. Seijo, *Theor. Chem. Acc.*, 2011, **129**, 545.
9 F. Cimpoesu, F. Dahan, S. Ladeira, M. Ferbinteanu and J.-P. Costes, *Inorg. Chem.*, 2012, **51**, 11279.
10 J. Paulovic, F. Cimpoesu, M. Ferbinteanu and K. Hirao, *J. Am. Chem. Soc.*, 2004, **126**, 3321.
11 M. Ferbinteanu, T. Kajiwara, K.-Y. Choi, H. Nojiri, A. Nakamoto, N. Kojima, F. Cimpoesu, Y. Fujimura, S. Takaishi and M. Yamashita, *J. Am. Chem. Soc.*, 2006, **128**, 9008.
12 S. Tanase, M. Ferbinteanu and F. Cimpoesu, *Inorg. Chem.*, 2011, **50**, 9678.
13 W. Koch and M. C. Holthausen, *A Chemist's Guide to Density Functional Theory*, Wiley-VCH, Berlin, 2001.
14 A. K. Theophilou, *J. Phys. C: Solid State Phys.*, 1979, **12**, 5419.
15 A. K. Theophilou and P. Papaconstantinou, *Phys. Rev. A: At., Mol., Opt. Phys.*, 2000, **61**, 022502.
16 A. Görling, *Phys. Rev. A: At., Mol., Opt. Phys.*, 1996, **54**, 3912.
17 M. E. Casida, *THEOCHEM*, 2009, **914**, 3.
18 F. Wang and T. Ziegler, *J. Chem. Phys.*, 2005, **122**, 074109.
19 J. C. Slater, *Adv. Quantum Chem.*, 1972, **6**, 1.
20 F. Neese, *JBIC, J. Biol. Inorg. Chem.*, 2006, **11**, 702.
21 J. S. Griffith, *The Theory of Transition Metal Ions*, Cambridge University Press, Cambridge, 1961.
22 B. N. Figgis and M. A. Hitchman, *Ligand Field Theory and its Applications*, Wiley-VCH, New York, 2000.
23 M. Atanasov, C. Daul and C. Rauzy, *Struct. Bonding*, 2004, **106**, 97.
24 M. Atanasov and C. Daul, *Chimia*, 2005, **59**, 504.
25 A. Borel and C. Daul, *THEOCHEM*, 2006, **762**, 93.
26 M. Atanasov, E. J. Baerends, P. Baettig, R. Bruyndonckx, C. Daul and C. Rauzy, *Chem. Phys. Lett.*, 2004, **399**, 433.
27 M. Atanasov and C. Daul, *C. R. Chim.*, 2005, **8**, 1421.
28 M. Atanasov, C. Daul, H. U. Güdel, T. A. Wesolowski and M. Zbiri, *Inorg. Chem.*, 2005, **44**, 2954.
29 L. Petit, A. Borel, C. Daul, P. Maldivi and C. Adamo, *Inorg. Chem.*, 2006, **45**, 7382.
30 A. Borel, L. Helm and C. Daul, *Chem. Phys. Lett.*, 2004, **383**, 584.
31 J. L. Sommerdijk, A. Bril and A. W. de Jager, *J. Lumin.*, 1974, **8**, 341.
32 W. W. Piper, J. A. DeLuca and F. S. Ham, *J. Lumin.*, 1974, **8**, 344.
33 D. Schiffbauer, C. Wickleder, G. Meyer, M. Kirm, M. Stephan and P. C. Schmidt, *Z. Anorg. Allg. Chem.*, 2005, **631**, 3046.
34 D. Tu, Y. Liu, H. Zhu, R. Li, L. Liu and X. Chen, *Angew. Chem., Int. Ed.*, 2013, **52**, 1128.
35 S. Hüfner, *Optical spectra of transparent rare earth compounds*, Academic Press, New York, 1978.
36 K. W. H. Stevens, *Proc. Phys. Soc. London, Sect. A*, 1952, **65**, 209.
37 C. Schäffer and C. Jørgensen, *Mol. Phys.*, 1965, **9**, 401.
38 E. Larsen and G. N. La Mar, *J. Chem. Educ.*, 1974, **51**, 633.
39 J. Sugar, *J. Opt. Soc. Am.*, 1965, **55**, 1058.
40 E. J. Baerends, T. Ziegler, J. Autschbach, D. Bashford, A. Bérces, F. M. Bickelhaupt, C. Bo, P. M. Boerrigter, L. Cavallo, D. P. Chong, L. Deng, R. M. Dickson, D. E. Ellis, M. van Faassen, L. Fan, T. H. Fischer, C. F. Guerra, A. Ghysels, A. Giammona, S. J. A. van Gisbergen, A. W. Götz, J. A. Groeneveld, O. V. Gritsenko, M. Grüning, S. Gusarov, F. E. Harris, P. van den Hoek, C. R. Jacob, H. Jacobsen, L. Jensen, J. W. Kaminski, G. van Kessel, F. Kootstra, A. Kovalenko, M. V. Krykunov, E. van Lenthe, D. A. McCormack, A. Michalak, M. Mitoraj, J. Neugebauer, V. P. Nicu, L. Noodleman, V. P. Osinga, S. Patchkovskii, P. H. T. Philipsen, D. Post, C. C. Pye, W. Ravenek, J. I. Rodríguez, P. Ros, P. R. T. Schipper, G. Schreckenbach, J. S. Seldenthuis, M. Seth, J. G. Snijders, M. Solà, M. Swart, D. Swerhone, G. te Velde, P. Vernooijs, L. Versluis, L. Visscher, O. Visser, F. Wang, T. A. Wesolowski, E. M. van Wezenbeek, G. Wiesenekker, S. K. Wolff, T. K. Woo and A. L. Yakovlev, *ADF2010.01*, available at http://www.scm.com.
41 C. F. Guerra, J. G. Sniders, G. te Velde and E. J. Baerends, *Theor. Chem. Acc.*, 1998, **99**, 391.
42 G. te Velde, F. M. Bickelhaupt, S. J. A. van Gisbergen, C. F. Guerra, E. J. Baerends, J. G. Sniders and T. Ziegler, *J. Comput. Chem.*, 2001, **22**, 932.
43 S. Vosko, L. Wilk and M. Nussair, *Can. J. Phys.*, 1980, **58**, 1200.

44 M. Swart, A. W. Ehlers and K. Lammertsma, *Mol. Phys.*, 2004, **102**, 2467.
45 P. J. Stephens, F. J. Devlin, C. F. Chabalowski and M. J. Frisch, *J. Phys. Chem.*, 1994, **98**, 11623.
46 G. Kresse and J. Hafner, *Phys. Rev. B: Condens. Matter Mater. Phys.*, 1993, **47**, 558.
47 W. A. Runciman and B. G. Wybourne, *J. Chem. Phys.*, 1959, **31**, 1149.
48 J. Sugar, *Phys. Rev. Lett.*, 1965, **14**, 731.
49 H. M. Crosswhite, G. H. Dieke and W. J. Carter, *J. Chem. Phys.*, 1965, **43**, 2047.
50 J.-F. Wyart, A. Meftah, J. Sinzelle, W.-Ü. L. Tchang-Brillet, N. Spector and B. R. Judd, *J. Phys. B: At., Mol. Opt. Phys.*, 2008, **41**, 085001.
51 R. T. Wegh, A. Meijerink, R. J. Lamminmäki and J. Hölsa, *J. Lumin.*, 2000, **87–89**, 1002.
52 W. C. Martin, R. Zalubas and L. Hagan, *Natl. Stand. Ref. Data Ser.*, 1978, (NSRDS-NBS 60), 422.
53 A. Kramida, Yu. Ralchenko and J. Reader, *NIST ASD Team*, 2012, http://physics.nist.gov/asd [2013, March 24th].
54 C. Schäffer and C. Jørgensen, *J. Inorg. Nucl. Chem.*, 1958, **8**, 143.
55 M. Atanasov, C. Daul and C. Rauzy, *Chem. Phys. Lett.*, 2003, **367**, 737.
56 R. D. Shannon, *Acta Crystallogr., Sect. A: Cryst. Phys., Diffr., Theor. Gen. Cryst.*, 1976, **32**, 751.
57 P. A. Tanner, V. V. R. K. Kumar, C. K. Jayasankar and M. F. Reid, *J. Alloys Compd.*, 1994, **215**, 349.
58 W. Urland, *Angew. Chem., Int. Ed. Engl.*, 1981, **20**, 210.
59 P. A. Tanner, C. S. K. Mak, M. D. Faucher, W. M. Kwok, D. L. Philips and V. Mikhailik, *Phys. Rev. B: Condens. Matter Mater. Phys.*, 2003, **67**, 115102.